Supplementary Materials for

Widespread synchronous decline in a Mediterranean forest driven by accelerated aridity

Materials and Methods

Methods

Study area

Mediterranean-type ecosystems (MTEs) are characterized mainly by their climate attributes viz. mild, wet winters and warm, dry summers, and by their vegetation structure, comprising plants with similar functional traits with analogous vegetation types (*31*). These ecosystems are highly diverse having different types of woodlands, scrubs, pasture lands and forests (*32*). However, the dominant vegetation is the typical sclerophyllous forest and shrubland, an analogous formation between the MTEs that is associated with high plant species diversity (*31*).

Five MTEs regions are recognized globally: South Africa, the Mediterranean Basin, California, Southwest Australia and central Chile (*31*). The boundaries of these regions are not consistently defined and depend on the delineation approach (*33*). To delineate these regions we combined two criteria: (1) areas classified as Csa or Csb by Köppen-Geiger, obtained from (*34*) as a 1-km-grid global map, and (2) arid and semi-arid areas worldwide using the Global Aridity Index (GAI = Mean Annual Precipitation/Mean Annual Reference Evapotranspiration), obtained from (*35*) (Fig. S1). The analysis was done for the forest area intersecting both datasets.

Climatic data and analysis

To provide a global scale depiction of the precipitation anomalies during the last decade (Fig. 1) we used the Global Precipitation Climatology Project monthly precipitation dataset (1979–present) combining observations and satellite precipitation data into 2.5°×2.5° grids (*36*). The anomalies are departures from the long term mean 1980–2010. For a more specific analyses of the precipitation and temperature anomalies in the MTEs we used the Climate Research Unit (CRU) TS dataset (release 4.04) for January 1901–December 2020 on a 0.5°×0.5° grid over landmasses (*37*). The CRU-TS dataset is derived using interpolation of monthly climate anomalies from extensive networks of weather station observations. Values for each MTEs (used for Figs. 1B and 2) are the area mean of the grid points within each MTEs bounding box.

The Standardized Precipitation Evapotranspiration Index (SPEI) was obtained from the SPEI Global Drought Monitor (https://spei.csic.es/) with monthly data from 1955 onwards available at 1°×1° grids over land domains. SPEI values for each MTEs (used for Fig. S2) are the area mean of the grid points within each MTEs bounding box.

To provide an estimate of the precipitation anomalies caused by climate change during the last decade, we considered the 2010–2020 precipitation anomalies from 26 GCMs comprising the Coupled Model Intercomparison Project - Phase 5 (CMIP5; (*38*)) and integrated them under the RCP8.5 scenario. Fig. 1B includes the multi-model mean anomalies that effectively isolates the signal due to anthropogenic climate forcing.

Forest change analysis

The evaluated forest was obtained from MCD12Q1 V6 MODIS 2000 Global Land Cover in the Google Earth Engine platform (GEE) (*39*), with a spatial resolution of 500 m. We considered four types of forests: (i) Evergreen Needleleaf Forests: dominated by evergreen conifer trees (canopy >2m) and tree cover >60%, (ii) Evergreen Broadleaf Forests: dominated by evergreen broadleaf and palmate trees (canopy >2m) and tree cover >60%, (iii) Mixed Forests: dominated by neither deciduous nor evergreen (40-60% of each) tree type (canopy >2m) and a tree cover >60%, and (iv) Woody Savannas: tree cover 30-60% (canopy >2m) (*40*). We excluded all the burned pixels within the 2000–2021 period using the monthly global burned area product MCD64A1.006 from MODIS (*41*). The code used in GEE is available here: https://code.earthengine.google.com/b90dc3d159b8be88dc8aa52308c227d7

Statistical analysis of time series

We applied a time series analysis to assess the changes that the forest has experienced during the last two decades. We used the Normalized Difference Vegetation Index (NDVI) data from the MOD13Q1 V6 product (also available in GEE). This global product allows the evaluation of NDVI every 16 days at a spatial resolution of 250 m.

To identify the trend of the time series of NDVI on each MTEs, we applied a modified Mann-Kendall test for autocorrelated data, which assesses statistical significance of the temporal changes (*28*). The analysis considered the period 21/06/2000–21/06/2021, wherein we assessed the magnitude of the trend via the Sen's slope test. The percentage of pixels with a significant negative trend was defined considering a p-value of 0.01. All analyses were done in the statistical software R version 4.0.5.

Date detection of forest decline

Considering the regional response of the forest in central Chile, we applied an additional analysis for those time series to detect the date on which each pixel collapsed. This helped us to assess how synchronous this event was. The forest canopy collapse was defined as the point in the time series where an abrupt change occurred. This was identified in two steps: I the preprocessing of the NDVI time series to remove outliers and missing data; II the estimation of the change-point date i.e. the point that partitions the series in two regions that minimize the sum of the residual (squared) error of each region from its local mean.

Let $y^{(j)} = \left(y_1^{(j)}, y_2^{(j)}, \dots, y_t^{(j)}, \dots, y_T^{(j)}\right)$ be the NDVI records in a pixel j, and T the number of elements, and/or last recorded date.

Step I:

- Detection and removal of outliers: the NDVI records that fall beyond 3 standard deviations from the NDVI mean are removed.
- Detection and removal of missing data: missing records in the NDVI series data are detected and removed.
- Interpolation of outliers and missing data: The outliers and missing points are replaced by the linear interpolation of the previous and immediate-post NDVI records.
- Fit a spline function (f) to the NDVI data corrected in the previous steps.

Step II:

- Find change-points in the NDVI series using the approximation $f(y^{(j)}) = (z_1^j, z_2^j, \dots, z_T^j)$, where f is the function spline and $z_i^j := f\left(y_i^{(j)}\right)$. The spline function f smoothens the NDVI records $y_i^{(j)}$, removing additional noise found in Step I.
- Select the change-point t^* so that it partitions the series z^j into two regions: $\left(z^j\right)_{1:t^*-1}$ and $(z^{(j)})_{t^*:T}$, that minimize the sum of the residual (squared) error of each region from its local mean. That is, t^* is the solution of the following optimization problem:

$$\min_{1\le t\le T} J^{(j)}(t) := \sum_{i=1}^{t-1}\left(z_i^j - mean\left[z_1^j, \dots, z_{t-1}^j\right]\right)^2 + \sum_{i=t}^{T}\left(z_i^j - mean\left[z_t^j, \dots, z_T^j\right]\right)^2.$$

Steps I and II are repeated for all series of each pixel, and the change-points t^* are recorded. All analyses were done in Matlab R2021b.

Vegetation field surveys

Field data was used as a descriptor of forest composition and productivity at a plot and individual scale to explore the trends towards forest canopy collapse. Individual-focused data from 474 trees (diameter >10 cm) of mesic species (i.e. *Cryptocarya alba–Peumus boldus*) and xeric species (i.e. *Quillaja saponaria–Lithraea caustica*), dominant in central Chile Mediterranean forests. Plot data included 78 circular samples (400 m^2) located in Coastal and Andean Range, and on the central valley.

To assess vegetation productivity, we used the Normalized Difference Vegetation Index (NDVI), and Leaf Area Index (LAI) as a proxy of plot and tree function, respectively. These variables reflect the tree's capacity to absorb energy for photosynthesis, maintain the leaves turgor and preserve the global energy balance in the canopy. Values for NDVI were calculated for each sample plot derived from Landsat 8 imagery (resolution 30 m). The NDVI at the plot level was calculated as the mean of the spring season NDVI. Values of LAI at the individual level were obtained from field measurements using a ceptometer (model DECAGON ACCUPAR LP-80).

Due the unusual drought condition during the spring-summer 2019 and its effect on tree canopy, we registered the percentage of the crown affected by browning for each individual. All data were measured for years 2017, 2019 and 2020 during the spring and summer seasons.

Supplementary Figures

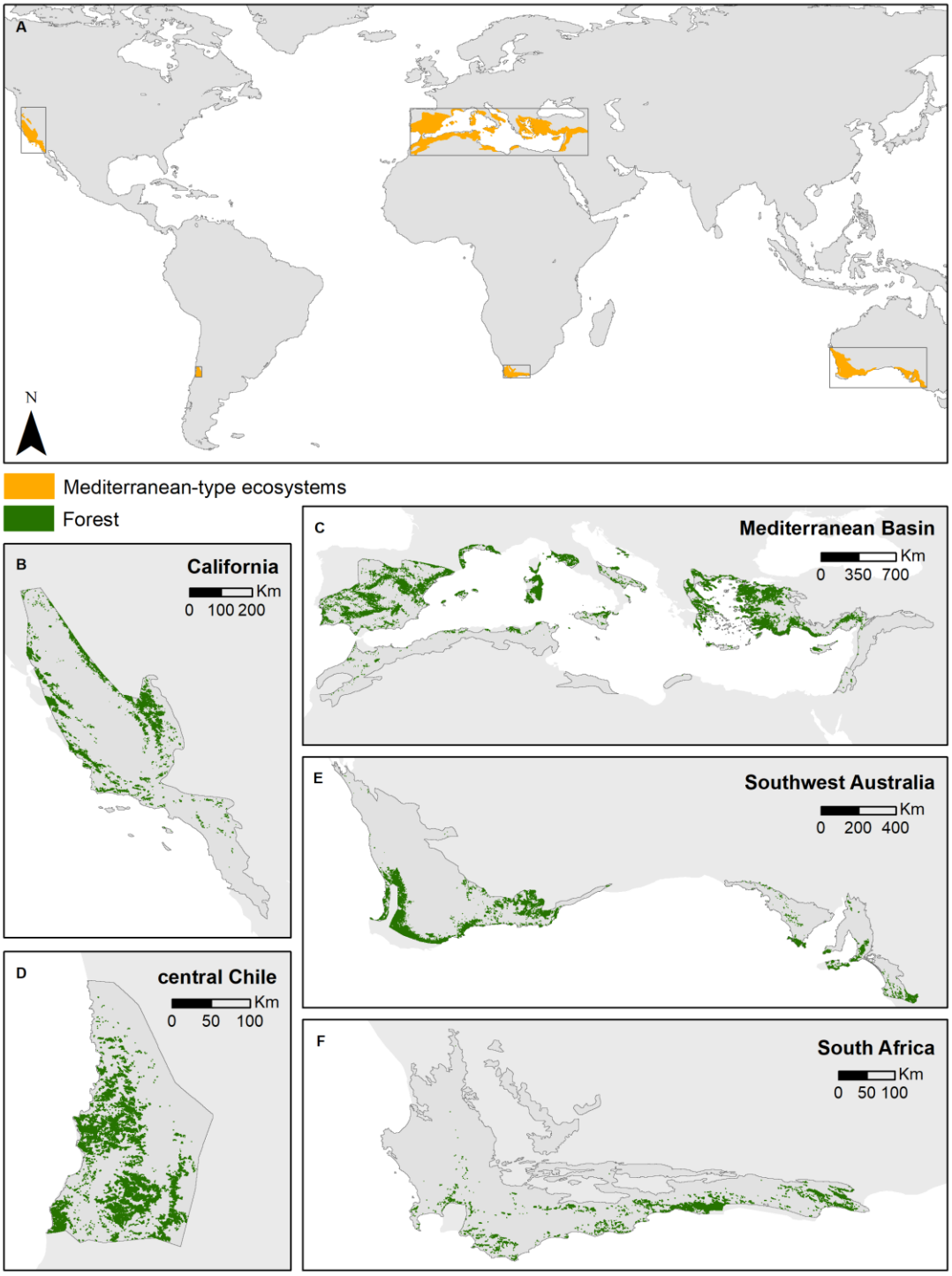


Figure S1. Mediterranean type Ecosystems. (**A**) Global distribution of the MTEs regions. The location of the forest within each region is presented in (**B**) California, (**C**) Mediterranean Basin, (**D**) central Chile, (**E**) Southwest Australia and (**F**) South Africa.

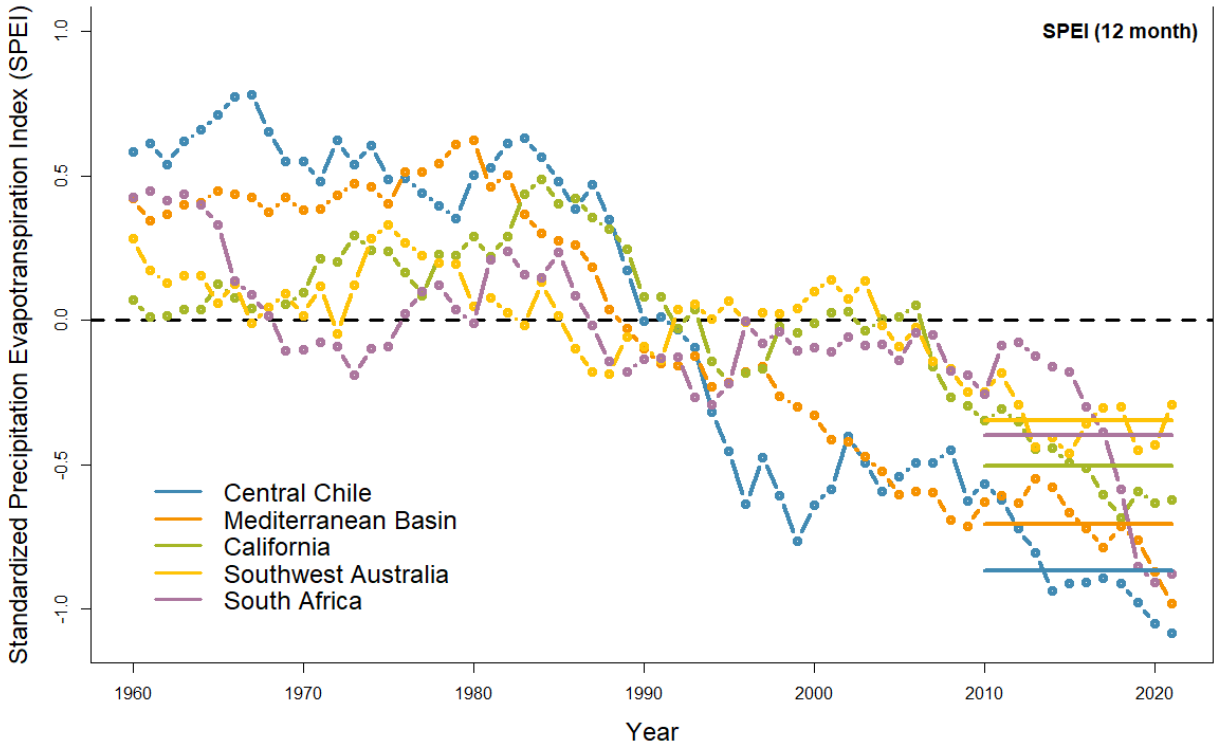
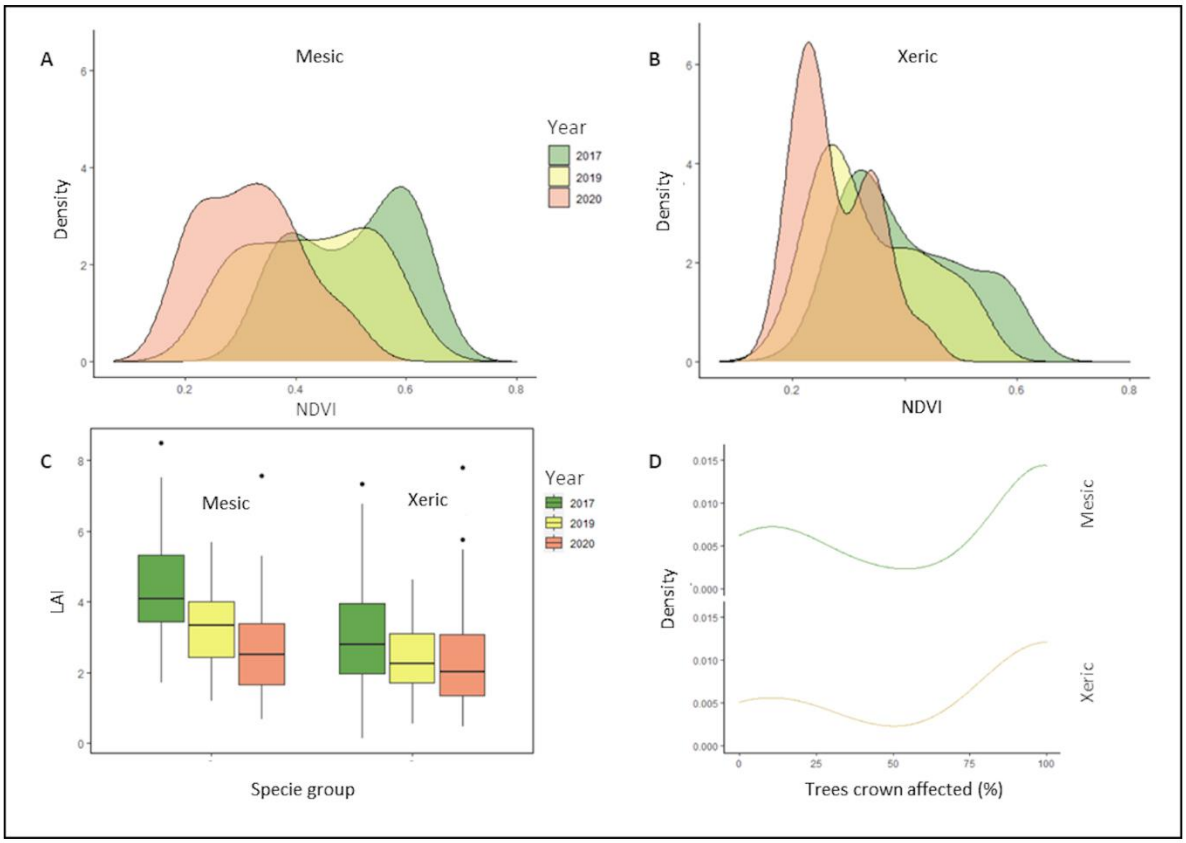


Figure S2. Surface water balance time series. Standardized Precipitation Evapotranspiration Index (SPEI-12) for each MTE for 1960–2021. Solid line between 2010 and 2021 indicates the mean SPEI-12 value for each MTE. Data from SPEI Drought Monitor (https://spei.csic.es/index.html).



157
158 **Figure S3:** Assessment of the variation in productivity and browning for xeric and mesic forests
159 of Central Chile MTE. Variation in productivity for years 2017, 2019 and 2020 at a 400m^2 plot for
160 (**A**) Mesic forests and (**B**) Xeric forests; (**C**) reflects the change in Leaf Area Index (LAI) at the
161 tree level for the years of analysis; (**D**) shows the estimated browning at tree level for 2019–2020.
162
163
164
165

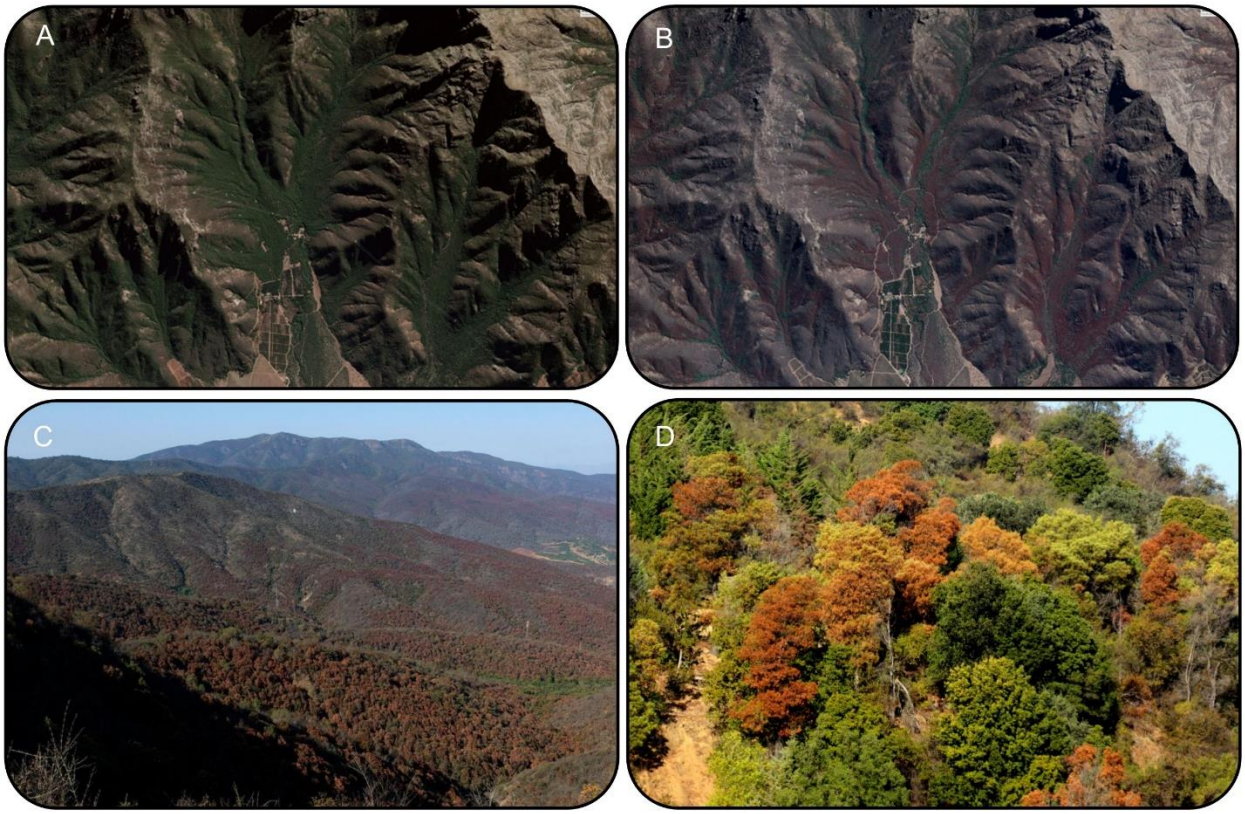


Figure S4. **Examples showing the magnitude decline in evergreen sclerophyllous forests in central Chile.** (**D** and **E**) Google Earth image from March 2019 and March 2020 from central Chile (5 km × 7 km image). (**F** and **G**) The sclerophyllous forest viewed at landscape and plot scale, respectively.

Table S1. Forest type and area for each Mediterranean type ecosystem.

MTE	Forest Area (km^2)	Evergreen Needleleaf (km^2)	Evergreen Broadleaf (km^2)	Mixed Forest (km^2)	Woody Savanna (km^2)	Negative trend (% forest)	Negative trend (km^2 forest)
Mediterranean Basin	76,492	25,085	4,843	3,622	47,976	1	765
Southwest Australia	22,843	197	3,218	362	34,290	6	1,370
South Africa	2,474	151	2,430	1	3,760	5.7	141
Central Chile	6,061	1,316	739	7	5,271	39	2,363
California	3,300	4,797	878	165	8,708	8.3	274

References

31. P. W. Rundel *et al.*, *Annu. Rev. Ecol. Evol. Syst.* **47**, 383–407 (2016).

32. E. Dinerstein *et al.*, *BioScience*. **67**, 534–545 (2017).

33. D. D. Ackerly, W. D. Stock, J. A. Slingsby, in *Fynbos*, N. Allsopp, J. F. Colville, G. A. Verboom, Eds. (Oxford University Press, 2014; https://oxford.universitypressscholarship.com/view/10.1093/acprof:oso/9780199679584.001.0001/acprof-9780199679584-chapter-16), pp. 361–376.

34. H. E. Beck *et al.*, *Sci. Data*. **5**, 180214 (2018).

35. A. Trabucco, R. Zomer, Global Aridity Index and Potential Evapotranspiration (ET0) Climate Database v2 (2019), p. 1705236666 Bytes, , doi:10.6084/M9.FIGSHARE.7504448.V3.

36. R. F. Adler *et al.*, *J. Hydrometeorol.* **4**, 1147–1167 (2003).

37. I. Harris, T. J. Osborn, P. Jones, D. Lister, *Sci. Data*. **7**, 109 (2020).

38. K. E. Taylor, R. J. Stouffer, G. A. Meehl, *Bull. Am. Meteorol. Soc.* **93**, 485–498 (2012).

39. N. Gorelick *et al.*, *Remote Sens. Environ.* **202**, 18–27 (2017).

40. Friedl, Mark, Sulla-Menashe, Damien, MCD12Q1 MODIS/Terra+Aqua Land Cover Type Yearly L3 Global 500m SIN Grid V006 (2019), , doi:10.5067/MODIS/MCD12Q1.006.

41. Giglio, Louis, Justice, Christopher, Boschetti, Luigi, Roy, David, MCD64A1 MODIS/Terra+Aqua Burned Area Monthly L3 Global 500m SIN Grid V006 (2015), , doi:10.5067/MODIS/MCD64A1.006.